On the harmonics of the low-frequency quasi-periodic oscillation in GRS 1915+105

E.M. Ratti[1]⋆, T.M. Belloni[2], S.E. Motta[2]

[1]*SRON, Netherlands Institute for Space Research, Sorbonnelaan 2, 3584 CA, Utrecht, The Netherlands*
[2]*INAF-Osservatorio Astronomico di Brera, via E. Bianchi 46, 23807 Merate (LC), Italy*

27 February 2013

ABSTRACT

GRS 1915+105 is a widely studied black hole binary, well known because of its extremely fast and complex variability. Flaring periods of high variability alternate with "stable" phases (the *plateaux*) when the flux is low, the spectra are hard and the timing properties of the source are similar to those of a number of black hole candidates in hard spectral state. In the *plateaux* the power density spectra are dominated by a low frequency quasi periodic oscillation (LFQPO) superposed onto a band limited noise continuum and accompanied by at least one harmonic. In this paper we focus on three *plateaux*, presenting the analysis of the power density spectra and in particular of the LFQPO and its harmonics. While plotting the LFQPO and all the harmonics together on a frequency-width plane, we found the presence of a positive trend of broadening when the frequency increases. This trend can shed light in the nature of the harmonic content of the LFQPO and challenges the usual interpretation of these timing features.

1 INTRODUCTION

X-ray binaries are binary systems where a stellar compact object, a neutron star (NS) or a black hole (BH) accretes matter from a companion star, producing bright X-ray emission. Since its launch in 1995, the *Rossi X-Ray Timing Explorer (RXTE)* has allowed a direct comparison between the spectral and timing properties of large sample of XRBs, which allowed the definition of the typical phenomenological properties of sources hosting a NS or a BH (see Psaltis 2006 for a review). On the base of those properties, quite a number of sources have been identified as possibly hosting a BH (black-hole candidates, BHC): for a number of systems this prediction has been confirmed via dynamical studies. Most BHCs have a low-mass companion star and are transient sources (black-hole transients, BHT) showing an evolution of their spectral/timing properties during their outbursts. This evolution has been described by many authors as a transition through a combination of 3-4 states (see Remillard & McClintock 2006 and Belloni 2010 for a review) mainly defined by the shape and features in the power density spectra (PDS) and by the hardness of the energy spectra. The typical PDS are composed by a band-limited noise continuum that varies during the outburst and by a number of quasi-periodic oscillations (QPOs) observed in association with certain states both at low (mHz to few tens of Hz) and high (tents to hundreds Hz) frequencies (van der Klis 2006). Various models have been proposed in order to explain the quasi periodic variability and the noise continuum (see van der Klis 2005 for a review, Ingram & Done 2011 for a more recent model) but none of them, at the present time, can

give a comprehensive explanation of all the observed phenomena.

In this paper we focus on the low frequency QPO (LFQPO) of GRS 1915+105. LFQPOs are common features in the PDS of BHTs (unlike high-frequency QPOs, with frequencies larger than $\sim$ 30 Hz, that are rather rare) during their hard spectral states. They appear as strong peaks at a centroid frequency between 0.01 and 15 Hz, with a fractional rms amplitude reaching values >15% in sources like XTE J1550−564 and GRS 1915+105 (Sobczak et al. 2000, Reig et al. 2000). LFQPOs are often accompanied by one or more further QPO peaks whose frequency is in harmonic relation with that of the LFQPO itself. Those are traditionally interpreted as resulting from the Fourier decomposition of the quasi-periodic signal responsible for the LFQPO. Nonetheless, questions about the identification of the fundamental peak and the genuineness of the harmonic relationship of the peaks have been raised in the recent works of Rao et al. (2010) and Rodriguez & Varnière (2011). With the aim of investigating the relation between the LFQPO and its harmonics, we analysed a sample of *RXTE* observations from GRS 1915+105, which is particularly favorable for this study due to the strength of the main QPO peak and the number of the harmonics. The source is a largely studied XRB (see Fender & Belloni 2004 for a review) with a K-M III (Greiner et al. 2001b) star donating matter to a dynamically confirmed BH (Greiner et al. 2001a). It was discovered as a transient source on August 15, 1992 by the *WATCH* instrument on board on the *GRANAT* satellite (Castro-Tirado et al. 1992) and since then it always remained bright in the

Table 1. List of the *RXTE*/PCA archival observations analysed in this paper. The observations are divided in three blocks, corresponding to the three subsequent *plateaux* in Fig. 1.

Obs	MJD (50000.0)	Counts (Crab units)
10408−01−22−01	275.2230	0.818
10408−01−22−02	275.3564	0.796
10408−01−23−00	278.4915	0.873
10408−01−24−00	280.1696	0.790
10408−01−25−00	283.4941	0.732
10408−01−27−00	290.5768	0.715
10408−01−28−00	298.5349	0.699
10408−01−29−00	305.3730	0.709
10408−01−30−00	313.3129	1.141
10408−01−31−00	320.1960	0.922
20402−01−04−00	415.1299	0.864
20402−01−05−00	421.9758	0.551
20402−01−07−00	436.6608	0.511
20402−01−08−00	441.9193	0.519
20402−01−08−01	442.1189	0.485
20402−01−09−00	448.2834	0.427
20402−01−10−00	455.9928	0.387
20402−01−11−00	462.0617	0.356
20402−01−12−00	471.0688	0.346
20402−01−13−00	477.8727	0.368
20402−01−14−00	480.8806	0.357
20402−01−15−00	488.7786	0.317
20402−01−16−00	501.8847	0.312
20402−01−18−00	512.8887	0.329
20402−01−19−00	517.0462	0.294
20402−01−20−00	524.9231	0.315
20402−01−21−00	533.8351	0.309
20402−01−49−00	729.3267	0.759
20402−01−49−01	730.3943	0.726
20402−01−50−01	737.4041	0.600
20402−01−51−00	743.2941	0.597
20402−01−52−00	746.5504	0.602

Figure 1. The *RXTE*/PCA observations analysed in this paper (black points) superimposed onto the *RXTE*/ASM daily−average light curve between October 1995 and December 1997 (from Belloni et al. (2000)). The flux level is different because of the different energy band of PCA and the ASM. PCA data belong to three *plateaux*, the middle one being significantly longer that the others.

Figure 2. The most general multi-Lorentzian model we applied to the PDS. The Lorentzian components are labeled according to Belloni et al. (2002). The L_{IV} component accounts for residuals in the fit in a few observations, but is never significant.

2   OBSERVATIONS AND DATA REDUCTION

We analysed a set of thirty-two *RXTE*/PCA observations from the *RXTE* NASA's archive (Table 1) performed between July 1996 and October 1997 during the three subsequent *plateaux* shown in Fig. 1 (for a more general studies of the same plateaux, Trudolyubov 2001).

Power Density Spectra (PDS) have been extracted in a $\sim 2 - 14$ keV energy band from PCA light curves (single bit data with temporal resolution $125\mu s$) with a Nyquist frequency of 2048 Hz, normalised according to Leahy et al. (1983) and converted to square fractional root mean square

X-ray sky ($\sim$ 0.5 - 2 Crab), undergoing an 18-year long outburst that at the time of writing is still ongoing. Starting from 1996, GRS 1915+105 has been monitored with *RXTE*. The light curve in Fig. 1 is an example of the long-scale behavior of the source: quiet periods of low flux and low variability lasting hours to tens of days (the *plateaux*, Fender et al. 1999), alternate with flaring activity phases of extreme variability, when all the X-ray properties, flux, spectral parameters and PDS features can vary on timescales down to the ms (Greiner et al. 1996, Belloni et al. 1997, Belloni et al. 2000). While peculiar and complex during the flaring phases, the behaviour of the source during the *plateaux* is similar to that of many other BHTs. In particular, the PDS show the typical band limited noise complex (extending up to ~ 100 Hz) and a strong LFQPO with several harmonics (Trudolyubov 2001, Reig et al. 2000). We analysed *RXTE* data from the three *plateaux* in Fig. 1: the data sample and the reduction method are described in Sect. 2, while the modeling of the PDS is described in Sect. 3. Sect. 4 presents our results, which are discussed in the final Sect. 5.
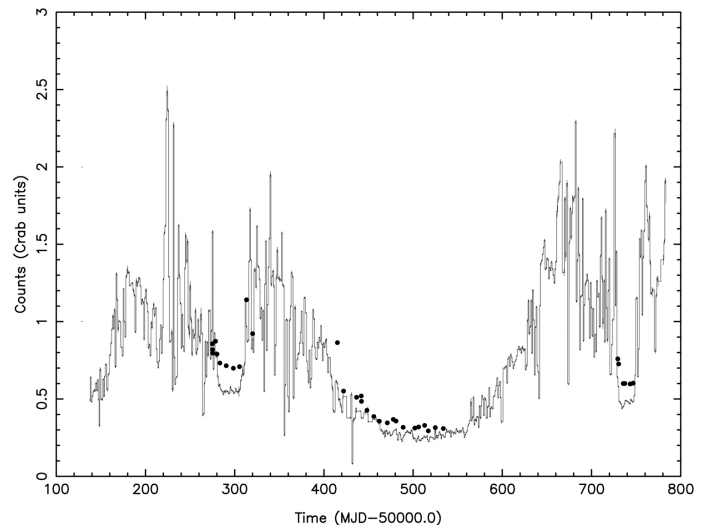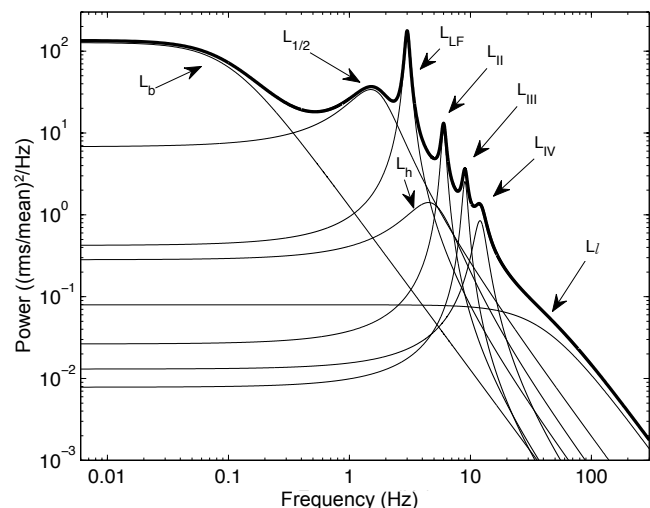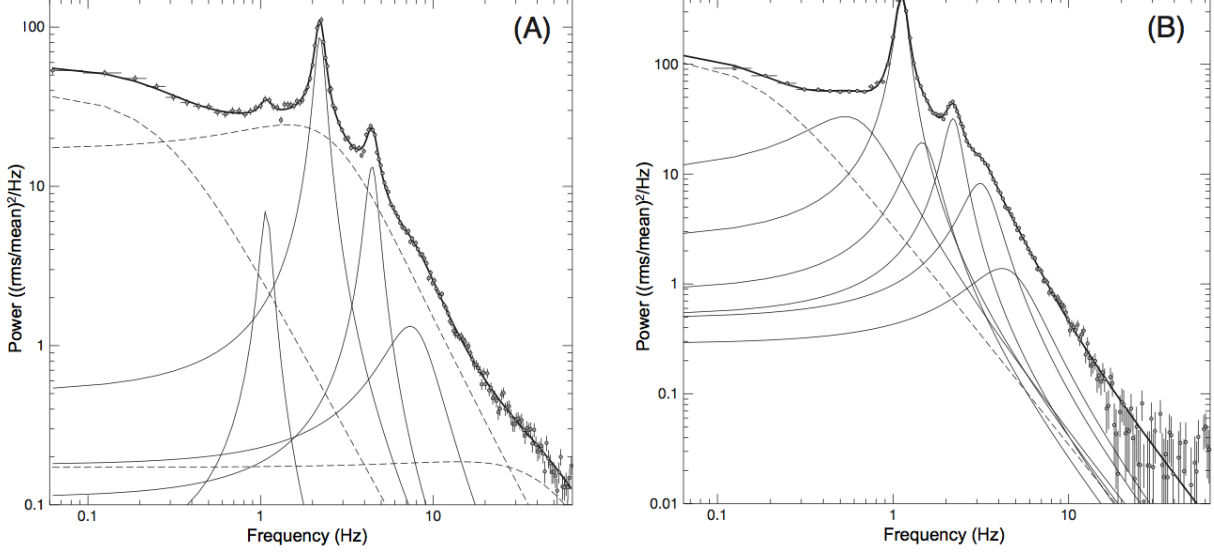
Figure 3. PDS from observation $20402-01-19-00$ (A) and $10408-01-27-00$(B) with our best fitting model. Continuum components are plotted as dashed lines, QPOs with filled lines. The high frequency component L_l (see Fig. 2) that is only observed during the long *plateau* (Trudolyubov 2001) can be seen in panel (A).

(rms) deviation (Belloni & Hasinger 1990). In order to improve the statistics, we obtained a PDS for each observation as the average of the Fourier spectra extracted from consecutive $16 - s$ segments of the light curve. The averaged PDS have been re-binned logarithmically in frequency and fitted with the standard XSPEC (version 11.3.2) fitting package using a diagonal response, therefore performing a simple direct χ^2 minimization. We adopted a model composed by Lorentzian functions only (see Fig. 2) following Belloni et al. (2002). As argued by the authors, this approach has the advantage that the spectrum is described by components that are directly comparable one to the other, with no assumption about the origin of each one. A component has been considered significant if $N/\sigma_N > 3$, where N is the normalisation and σ_N its uncertainty, obtained with the chi-squared minimization. The errors on individual powers of the fitted PDS were computed following van der Klis (1989). We accounted for the counting statistic in PDS using an automatic subtraction of Poissonian background, based on the estimate of PCA dead time by Zhang et al. (1995). A flat component extending over all the frequencies appears in a few PDS as a result of a non-perfect Poissonian subtraction. We corrected for this effect while fitting the PDS.

3   MULTI-LORENTZIAN MODELING OF THE PDS

Figure 3 shows two examples from the sample of PDS we analysed and the associated best-fitting model. Depending on the observation, five to eight Lorentzians are required for a good fit ($\chi^2 < 1.4$). We interpret each Lorentzian as a different spectral component (with the exception of double peaked QPOs, see below) assigning labels as in Fig. 2. We define the frequency ν and width Δ of a component as the central frequency and the FWHM of the associated Lorentzian function.

One to three Lorentzian components account for the band

limited continuum (see Fig. 2 and 3): a low frequency one, L_b, appears in 29 over 32 observations at $\nu_b \lesssim 0.2\ Hz$. L_h is often required at a centroid frequency ν_h, approximately located under the LFQPO L_{LF}. A high frequency component L_l only appears in observations from the longest *plateau* in Fig. 1, at $\nu_l \gtrsim 42\ Hz$. For a study of this component and its connection with "short" and "long" *plateaux*, see Trudolyubov 2001.

One Lorentzian is usually enough to fit the LFQPO peak, unless it happens to be double-peaked. The presence of a double peak is possible because the QPO is known to drift in frequency on time scales shorted than the average observation (see e.g. Markwardt et al. 1999). When this is the case, we fit two Lorentzians to the QPO and we take the sum-function as a single spectral component L_{LF} to represent the LFQPO. We consider the frequency of the most significant (larger %rms) peak as the frequency of L_{LF}, ν_{LF} and define its width Δ_{LF} as the FWHM of the sum-function of the overlapping Lorentzians. The error on Δ_{LF} is analytically computed from the equation of the sum-function. The quality factor $Q = \nu/\Delta$ (typical indicator for the coherence of a signal, a QPO is traditionally defined by $Q > 2$) of L_{LF} is always above 3, reaching a maximum value of 10.4 (see Table 2).

Although this is not the main topic of this paper, it is worth to mention that our data are consistent with the relations between ν_h, ν_l and ν_{LF} found in Belloni et al. (2002) for a sample of sources not including GRS 1915+105.

After fitting for the main QPO peak and the broad band-limited noise components L_b, L_h and L_l, further peaks or bumps in the PDS are best fitted by up to three components in harmonic relation with L_{LF}, labeled L_{II}, L_{III} and $L_{1/2}$. Their central frequencies are $\nu_{II} \sim 2\nu_{LF}$, $\nu_{III} \sim 3\nu_{LF}$ and $\nu_{1/2} \sim 0.5\nu_{LF}$ respectively. In three observations a further component (L_{IV} in Figure 2) needs to be added to our model in order to take into account residuals in the fit, whose centroid frequency is consistent with $\sim 4\nu_{LF}$. How-
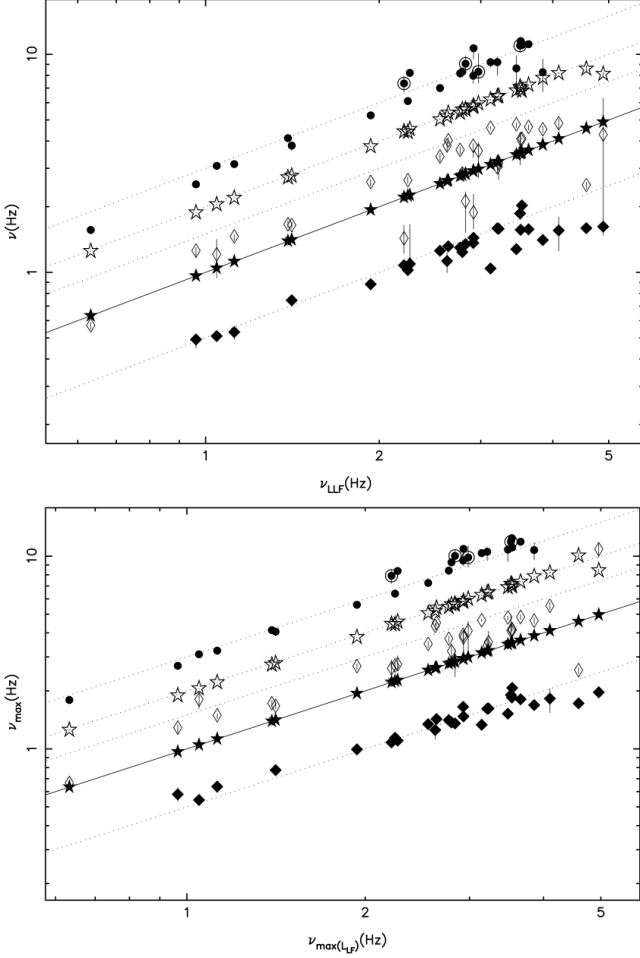
Figure 4. Top panel: Central frequency of L_{LF} (black stars), L_{II} (empty stars), L_{III} (black circles), $L_{1/2}$ (black diamonds) and L_h (empty diamonds) versus the frequency of L_{LF}. The black circles in an empty frame are 2 σ detections of L_{III}. Lines of constant ratio R= 0.5, 1, 1.5, 2 and 3 are plotted: the solid line is R=1. Bottom panel: same as top panel, but the characteristic frequency $\nu_{max} = \sqrt{\nu^2 + (\Delta/2)^2}$ is plotted instead of ν.

ever, this component never results significant (slightly less than 2σ detection) and therefore we did not consider it in our subsequent analysis. The component L_{II} always appear as a rather coherent peak, with $2 \lesssim Q \lesssim 10$. L_{III} and $L_{1/2}$ instead are often broad, with Q ranging from less than 1 up to $\sim$8 (see Table 3, 4, 5).

3.1 Harmonic relations

Figure 4 (top panel) shows the frequencies ν_{II}, ν_{III}, ν_{LF}, $\nu_{I/2}$ and ν_h plotted against the corresponding ν_{LF} (the data are reported in the tables from 2 to 6). The harmonic relation between the L_{LF} and L_{II} is evident from the figure. Quite some scattering is observed instead in the case of the broader components L_{III} and $L_{1/2}$, with a tendency of the points to lie slightly below the harmonic relation line. Figure 4 (bottom panel) suggests that the harmonic ratio is better represented for L_{III} and $L_{1/2}$ if we consider, instead of the frequency of the components, their 'characteristic frequency' $\nu_{max} = \sqrt{\nu^2 + (\Delta/2)^2}$ (Belloni et al. 2002). This is

a measure for the break frequency of a broad Lorentzian and around this frequency the component contributes most of its power per logarithmic frequency interval[1] (Belloni et al. 2002). When considering ν (upper panel of Fig. 4), a fit to the L_{III} and $L_{1/2}$ data-points with a line of constant ratio $\nu = A\nu_{LF}$ gives $A = 2.91 \pm 0.02$ ($\chi^2 = 131.2$, 24 d.o.f) and $A = 0.455 \pm 0.004$ ($\chi^2 = 412.3$, 27 d.o.f) for the two components respectively. The fitted slope is inconsistent with the expected harmonic ratios between the frequency of the each component and that of the L_{LF}. If we consider ν_{max} instead (Fig. 4 bottom panel), the fit gives $A = 3.00 \pm 0.02$ for L_{III} ($\chi^2 = 116.4$, 24 d.o.f) and $A = 0.49 \pm 0.004$ for $L_{1/2}$ ($\chi^2 = 191.4$, 27 d.o.f). In this case, the fitted slope is consistent with the expected harmonic ratios on the 1σ level for L_{III} and on the 3σ level for $L_{1/2}$. Although the fits are poor due to the scatter between the data-points, they support the visual impression given by Fig. 4 that the harmonic ratio of the L_{III} and $L_{1/2}$ is better represented when ν_{max} is used instead of ν.

The frequency of L_h is included in Figure 4 following a recent study of the PDS of XTE J1550-564 performed by Rao et al. (2010). The authors found that the ν_{max} of the component L_h (named L_{pn} by the authors) is in a 3/2 ratio with $\nu_{max(LF)}$, being at three times the characteristic frequency of the sub-harmonic $L_{1/2}$. We find that, in the case of GRS 1915+105, $\nu_{max(h)}$ lies slightly below the line indicating a constant ratio R=3/2 with $\nu_{max(LF)}$ (Figure 4 bottom panel). As L_h is a rather broad component, this discrepancy is even stronger if we consider the centroid frequencies ν_h and ν_{LF} (Figure 4 top panel).

4 HARMONICS IN A WIDTH-FREQUENCY PLANE

Fig. 5 shows the width of the L_{LF} and its higher order harmonics L_{II} and L_{III} plotted against the centroid frequency of the L_{LF}. The three components describe three clear tracks on the diagram, and the width of each component grows with frequency. Moreover, it seems that the highest is the order of the harmonic, the broader the peak is. Nonetheless, a different interpretation arises when considering the plot of Fig. 6, which provides a deeper insight on the behaviour of the harmonics. Here L_{LF}, L_{II} and L_{III} are considered again on a width-frequency plane, but the width Δ of each component is plotted against its own frequency ν, without implying a relation with the L_{LF} (the data are reported in the tables from 2 to 6). Lines of constant quality factor Q are also plotted. Different symbols distinguish harmonics of different orders, with the same key used in Fig. 5. With the exception of a few outliers, all points follow the same trend on this plot, where coherence decreases as centroid frequency increases. The harmonics can not be distinguished based on their width, as the tracks from different harmonics overlap one with another. Rather than depend on the order of the harmonic, a given Δ seems to be associated with a given frequency. A similar trend is observed if ν_{max} is plotted instead of ν.

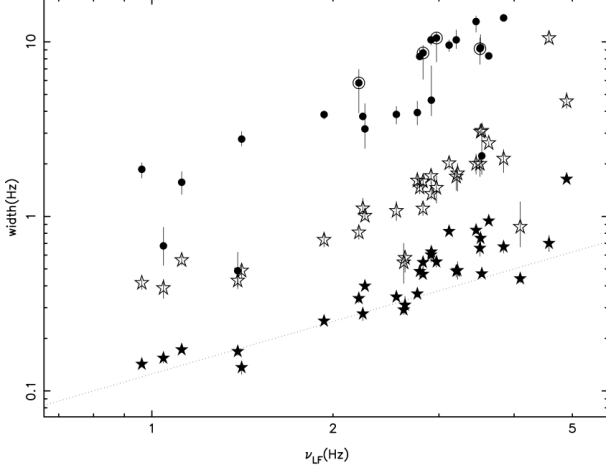[1] Note that ν_{max} becomes equal to ν for narrow components.

Figure 5. For each L_{LF} (black stars), L_{II} (empty stars) and L_{III} (black dots) detection, the width is plotted against the centroid frequency of the L_{LF} in the same PDS. The black dots in a white frame are 2 σ detections consistent with L_{III}. The dashed line shows the slope of a constant quality factor (Q=10) trend.

The relation between the quality factors of the different harmonics of a non-sinusoidal signal is determined by the nature of the quasi-periodicity of the signal. The width-frequency plots in Fig. 7 have been produced by assuming the ν of each harmonic peak in our data and calculating the expected Δ in case of a purely frequency - or purely amplitude - modulated signal. For a purely amplitude modulation, the Δ of all the harmonic peaks would be the same as the amplitude of the L_{LF}. On a frequency-width diagram that would result in a series of parallel tracks, one per each harmonic as shown in Fig. 7 panel (a). The diagram is clearly different than that resulting from the real data in Fig. 6. In the case of a frequency modulation, all the peaks have the same quality factor, that of the L_{LF}. This case is shown in Fig. 7 panel (b), which again is not consistent with the real data: although a single track is formed, it remains parallel to the $Q = const$ lines, not reproducing the curved shape that appears in the real GRS 1915+105 data set. A width-frequency diagram consistent with a pure frequency modulation was found instead for XTE J1550-564 (Rao et al. 2010).

The frequency-width diagram for components $L_{1/2}$ and L_h is shown in Fig. 8. A comparison of Fig. 8 and 6 shows that $L_{1/2}$ and L_h do not share the behaviour of the other harmonics.

5 DISCUSSION AND CONCLUSIONS

We have analysed the PDS of GRS 1915+105 during three *plateaux* states. The overall shape of the PDS is that typical of BHTs in their hard-intermediate state, with a strong low frequency QPO peak L_{LF} superimposed to a band limited noise continuum (Fig. 3, 2). The spectra can be fitted with a combination of Lorentzian components, several of which are in harmonic relation with L_{LF}. We detected up to two higher order harmonics (L_{II} and L_{III}) forming an harmonic series of 1:2:3 with L_{LF}, plus the components $L_{1/2}$ and L_h with frequency close to ~ 0.5 and ~ 1.5 times the frequency of the L_{LF} respectively. Few observations show residuals at

frequency consistent to $\sim 4L_{LF}$, but a further Lorentzian component added at this frequency never results significant above 2σ.

In the case of XTE J1550-564, Rao et al. (2010) proposed $L_{1/2}$ as the fundamental frequency of an harmonic 1:2:3:4 series including $L_{1/2}$, L_{LF}, L_h and L_{II}. In a similar scenario for GRS 1915+105, L_{III} should also be included, leading to a 1:2:3:4:6 series. Nonetheless, there is no strong evidence of a 2/3 harmonic ratio between the frequency of the L_{LF} and of L_h in the case of GRS 1915+105, even when the characteristic frequency of the components ν_{max} is considered in place of ν. Moreover, the plot in Figure 6 (which is not significantly affected by the choice of ν or ν_{max}) indicates that L_{LF} and its higher order harmonics are related beyond their frequency ratio as they broaden and lose coherence together as their frequency increases, while $L_{1/2}$ and L_h behave differently (Fig. 8) as if they did not belong to the L_{LF} harmonic series. We conclude that the $L_{1/2}$ is likely not the fundamental in the L_{LF} harmonic series, i.e. is not included in the series itself. $L_{1/2}$ and L_h could instead be produced by a different phenomenon than that responsible for the L_{LF}. Although the plot in Fig. 6 evidences a relation between L_{LF} and its higher order harmonics L_{II} and L_{III}, it also rises doubts on the nature of this relation. The commonly accepted idea is that the L_{LF} and the harmonics describe together the same signal from a quasi-periodic oscillator, appearing as separated peaks in the PDS as a consequence of the Fourier representation. However, it is not trivial to identify a signal modulation that is able to produce the trend in Fig. 6. For example, we have shown that such a behavior cannot be reproduced by a simple combination of frequency or amplitude modulation. Moreover, Fig. 4 shows that the frequency of L_{III} across different observations is better distributed around an harmonic ratio of 3 with the frequency of L_{LF} when considering ν_{max} instead of ν [2]. This is not what is usually expected in the context of harmonic decomposition, where the centroid ν is the frequency expected to be in harmonic ratio with the fundamental frequency. A broad component whose ν_{max} is in harmonic ratio with the fundamental frequency can not be regarded as a proper harmonic, but only as a signal whose characteristic frequency is consistent with an harmonic of the fundamental frequency. The complexity of these results invites to consider a scenario involving more than one real oscillator, where a physical phenomenon is triggering oscillations at multiple frequencies in the accretion disk or in the corona, each one resulting in an harmonic component of the PDS. The trigger could be such that the life time (i.e. the coherence) of each oscillator is determined only by its own frequency, in agreement with the the trend in Fig. 6. This toy-model example gives a feeling of the new perspectives that would be opened in the interpretation of the PDS if the harmonics were proven to have a meaning beyond the Fourier representation of a single quasi-periodic signal. Either way, the interpretation of the width-frequency plane of GRS 1915+105 promises to offer new insights on the QPO generation phenomenon in this system and in other XRBs.

---

[2] Note that, because L_{LH} is narrow, there is no significant difference between ν_{max} and ν for this component. The same holds for L_{II}.
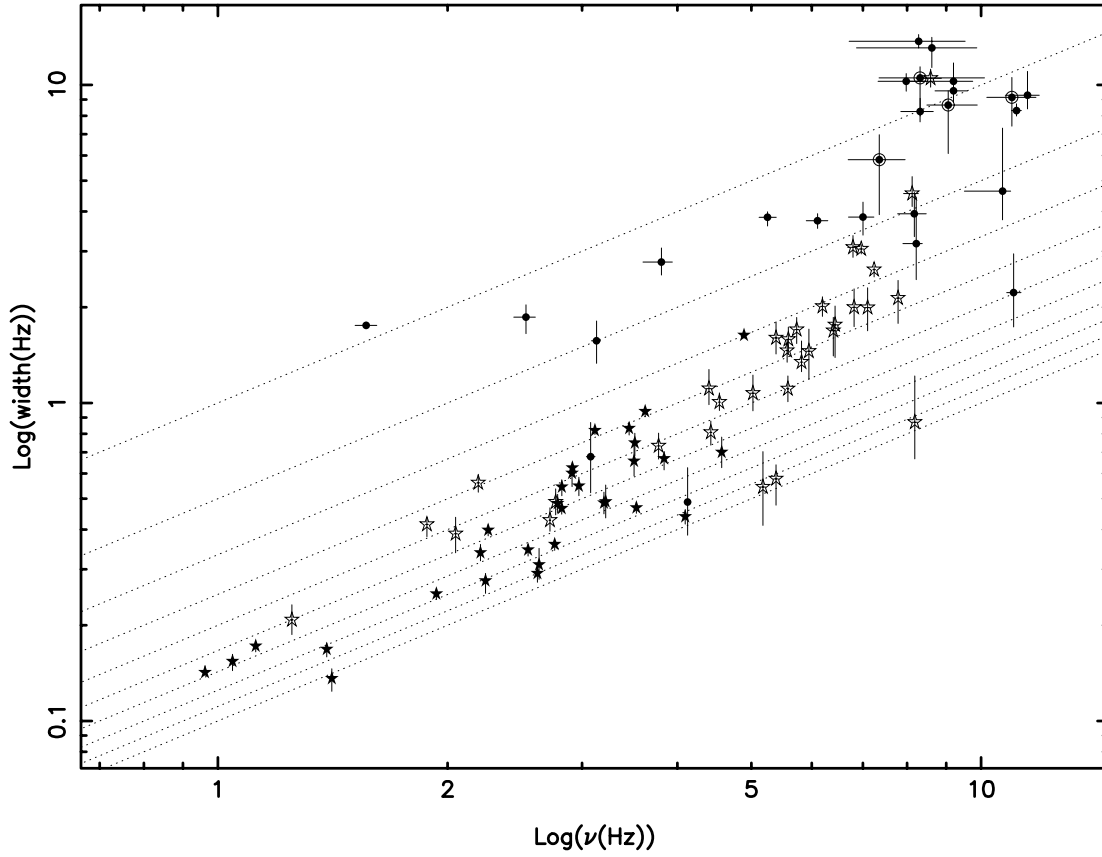
Figure 6. Harmonics on a width-frequency plane. Symbols are the same as in Figure 5: for each L_{LF} (black stars), L_{II} (empty stars) and L_{III} (black dots) component detected in the PDS, the width is plotted against the centroid frequency. The black dots in a white frame are 2 σ detections consistent with L_{III}. Lines of constant quality factor $Q = \nu/\Delta$ are plotted (dashed lines, Q increasing from 1 to 10 going from top to bottom).

(a)   (b)

Figure 7. Panels (a) and (b) show how the plot in Fig. 6 would look like in case the harmonics origin from a signal modulated in amplitude and frequency respectively. The points have the same frequency as the real data, but the width of each harmonic is : (a) the same as the width of the L_{LF} in the same observation (amplitude modulation) (b) calculated in order to obtain a constant Q for all the harmonics from the same PDS (frequency modulation).

Figure 8. Width versus centroid frequency (same as Fig. 6) for the sub-harmonic $L_{1/2}$ (black diamonds) and the component L_h (empty diamonds). Lines of constant quality factor $Q = \nu/\Delta$ are plotted as in Fig. 6 (dashed lines, Q increasing from 1 to 10 from top to bottom)
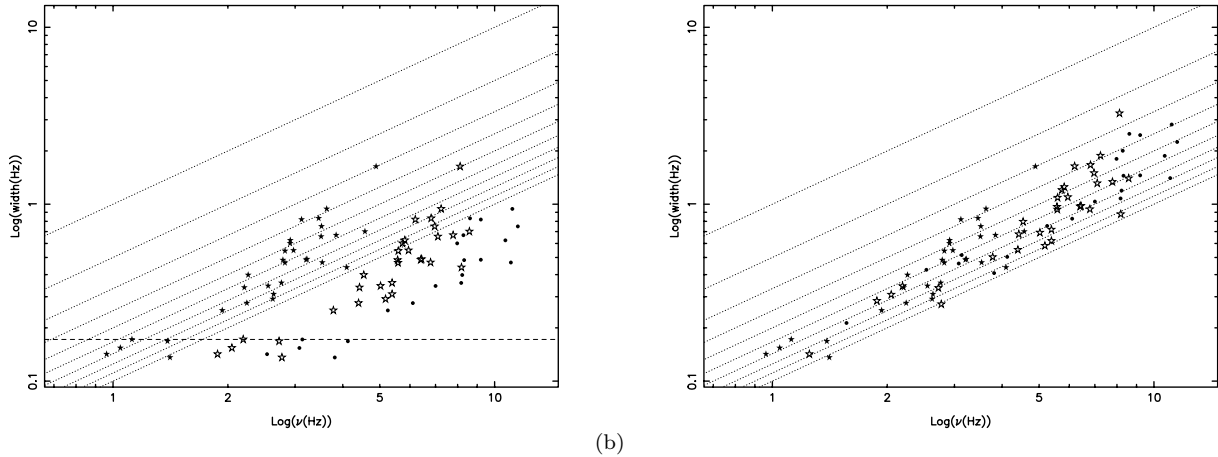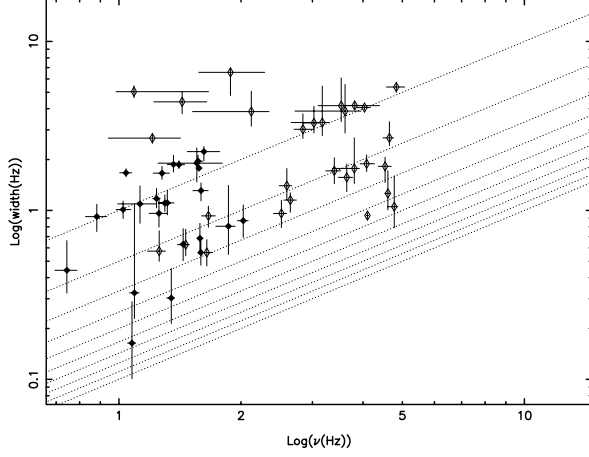
ACKNOWLEDGMENTS

Obs ID	ν_{LLF}	Δ_{LLF}
10408-01-22-01	$2.762\,^{+0.005}_{-0.006}$	$0.359^{+0.007}_{-0.015}$
10408-01-22-02	$2.549\,^{+0.005}_{-0.006}$	$0.345^{+0.014}_{-0.015}$
10408-01-23-00	$3.535\,^{+0.007}_{-0.007}$	$0.468^{+0.019}_{-0.018}$
10408-01-24-00	$2.242\,^{+0.005}_{-0.010}$	$0.276^{+0.015}_{-0.024}$
10408-01-25-00	$1.121\,^{+0.002}_{-0.003}$	$0.172^{+0.005}_{-0.007}$
10408-01-27-00	$0.632\,^{+0.002}_{-0.002}$	$0.071^{+0.005}_{-0.004}$
10408-01-28-00	$0.962\,^{+0.002}_{-0.002}$	$0.142^{+0.007}_{-0.003}$
10408-01-29-00	$1.933\,^{+0.003}_{-0.004}$	$0.251^{+0.009}_{-0.010}$
10408-01-30-00	$4.891\,^{+0.010}_{-0.010}$	$1.632^{+0.034}_{-0.034}$
10408-01-31-00	$4.095\,^{+0.006}_{-0.007}$	$0.439^{+0.023}_{-0.023}$
20402-01-04-00	$4.572\,^{+0.021}_{-0.025}$	$0.700^{+0.081}_{-0.074}$
20402-01-05-00	$2.822\,^{+0.004}_{-0.005}$	$0.466^{+0.020}_{-0.019}$
20402-01-07-00	$3.119\,^{+0.006}_{-0.006}$	$0.819^{+0.022}_{-0.023}$
20402-01-08-00	$3.843\,^{+0.011}_{-0.010}$	$0.668^{+0.035}_{-0.052}$
20402-01-08-01	$3.458\,^{+0.010}_{-0.011}$	$0.832^{+0.038}_{-0.039}$
20402-01-09-00	$2.823\,^{+0.007}_{-0.007}$	$0.544^{+0.029}_{-0.033}$
20402-01-10-00	$2.914\,^{+0.006}_{-0.006}$	$0.625^{+0.026}_{-0.024}$
20402-01-11-00	$2.911\,^{+0.008}_{-0.009}$	$0.601^{+0.036}_{-0.055}$
20402-01-12-00	$2.787\,^{+0.006}_{-0.007}$	$0.483^{+0.033}_{-0.032}$
20402-01-13-00	$3.630\,^{+0.007}_{-0.008}$	$0.940^{+0.023}_{-0.035}$
20402-01-14-00	$3.518\,^{+0.013}_{-0.016}$	$0.749^{+0.054}_{-0.067}$
20402-01-15-00	$2.260\,^{+0.005}_{-0.004}$	$0.398^{+0.016}_{-0.016}$
20402-01-16-00	$2.972\,^{+0.008}_{-0.009}$	$0.548^{+0.036}_{-0.037}$
20402-01-18-00	$3.222\,^{+0.011}_{-0.011}$	$0.489^{+0.063}_{-0.054}$
20402-01-19-00	$2.208\,^{+0.005}_{-0.005}$	$0.338^{+0.021}_{-0.019}$
20402-01-20-00	$3.205\,^{+0.007}_{-0.007}$	$0.485^{+0.039}_{-0.037}$
20402-01-21-00	$3.510\,^{+0.012}_{-0.013}$	$0.656^{+0.109}_{-0.067}$
20402-01-49-00	$2.622\,^{+0.006}_{-0.007}$	$0.291^{+0.019}_{-0.018}$
20402-01-49-01	$2.635\,^{+0.011}_{-0.014}$	$0.310^{+0.039}_{-0.031}$
20402-01-50-01	$1.045\,^{+0.002}_{-0.004}$	$0.154^{+0.008}_{-0.010}$
20402-01-51-00	$1.389\,^{+0.002}_{-0.003}$	$0.168^{+0.008}_{-0.009}$
20402-01-52-00	$1.410\,^{+0.003}_{-0.005}$	$0.136^{+0.010}_{-0.012}$

Table 2. Frequency ν_{LLF}, width Δ_{LLF} of the low frequency QPO L_{LF} from the best fit to the PDS.

Obs ID	ν_{II}	Δ_{II}
10408-01-22-01	$5.386^{+0.051}_{-0.057}$	$1.601^{+0.198}_{-0.175}$
10408-01-22-02	$5.024^{+0.036}_{-0.038}$	$1.073^{+0.151}_{-0.128}$
10408-01-23-00	$6.794^{+0.079}_{-0.106}$	$3.087^{+0.273}_{-0.217}$
10408-01-24-00	$4.399^{+0.025}_{-0.035}$	$1.110^{+0.164}_{-0.122}$
10408-01-25-00	$2.194^{+0.009}_{-0.010}$	$0.561^{+0.035}_{-0.037}$
10408-01-27-00	$1.250^{+0.005}_{-0.006}$	$0.208^{+0.024}_{-0.021}$
10408-01-28-00	$1.879^{+0.008}_{-0.008}$	$0.415^{+0.020}_{-0.035}$
10408-01-29-00	$3.780^{+0.020}_{-0.021}$	$0.733^{+0.071}_{-0.067}$
10408-01-30-00	$8.121^{+0.154}_{-0.206}$	$4.555^{+0.596}_{-0.408}$
10408-01-31-00	$8.186^{+0.066}_{-0.067}$	$0.870^{+0.346}_{-0.203}$
20402-01-04-00	$8.586^{+0.286}_{-0.358}$	$10.492^{+0.717}_{-0.650}$
20402-01-05-00	$5.582^{+0.019}_{-0.010}$	$1.108^{+0.108}_{-0.099}$
20402-01-07-00	$6.195^{+0.039}_{-0.037}$	$2.012^{+0.145}_{-0.140}$
20402-01-08-00	$7.784^{+0.051}_{-0.043}$	$2.137^{+0.291}_{-0.358}$
20402-01-08-01	$6.817^{+0.048}_{-0.047}$	$1.998^{+0.286}_{-0.260}$
20402-01-09-00	$5.590^{+0.039}_{-0.031}$	$1.585^{+0.146}_{-0.160}$
20402-01-10-00	$5.818^{+0.022}_{-0.023}$	$1.344^{+0.222}_{-0.090}$
20402-01-11-00	$5.733^{+0.041}_{-0.038}$	$1.702^{+0.155}_{-0.164}$
20402-01-12-00	$5.570^{+0.026}_{-0.026}$	$1.462^{+0.115}_{-0.119}$
20402-01-13-00	$7.242^{+0.031}_{-0.030}$	$2.626^{+0.069}_{-0.134}$
20402-01-14-00	$6.966^{+0.046}_{-0.049}$	$3.049^{+0.095}_{-0.107}$
20402-01-15-00	$4.541^{+0.015}_{-0.059}$	$1.006^{+0.070}_{-0.059}$
20402-01-16-00	$5.949^{+0.046}_{-0.057}$	$1.454^{+0.253}_{-0.267}$
20402-01-18-00	$6.437^{+0.056}_{-0.053}$	$1.761^{+0.257}_{-0.371}$
20402-01-19-00	$4.424^{+0.015}_{-0.015}$	$0.808^{+0.069}_{-0.071}$
20402-01-20-00	$6.403^{+0.034}_{-0.035}$	$1.688^{+0.171}_{-0.283}$
20402-01-21-00	$7.100^{+0.061}_{-0.065}$	$1.995^{+0.307}_{-0.309}$
20402-01-49-00	$5.178^{+0.040}_{-0.043}$	$0.544^{+0.159}_{-0.132}$
20402-01-49-01	$5.387^{+0.035}_{-0.038}$	$0.577^{+0.062}_{-0.100}$
20402-01-50-01	$2.049^{+0.011}_{-0.010}$	$0.388^{+0.049}_{-0.050}$
20402-01-51-00	$2.723^{+0.007}_{-0.008}$	$0.428^{+0.040}_{-0.033}$
20402-01-52-00	$2.771^{+0.012}_{-0.013}$	$0.488^{+0.049}_{-0.043}$

Table 3. Frequency ν_{II}, width Δ_{II} of the harmonic QPO L_{II} from the best fit to the PDS.

Obs ID	ν_{III}	Δ_{III}
10408-01-22-01	$8.176^{+0.298}_{-0.401}$	$3.936^{+0.654}_{-0.603}$
10408-01-22-02	$7.002^{+0.234}_{-0.299}$	$3.841^{+0.439}_{-0.470}$
10408-01-23-00	$11.030^{+0.249}_{-0.228}$	$2.224^{+0.721}_{-0.490}$
10408-01-24-00	$6.105^{+0.192}_{-0.204}$	$3.742^{+0.197}_{-0.204}$
10408-01-25-00	$3.135^{+0.037}_{-0.048}$	$1.569^{+0.241}_{-0.236}$
10408-01-27-00	$1.564^{+0.051}_{-0.051}$	$1.754^{+0.039}_{-0.021}$
10408-01-28-00	$2.533^{+0.073}_{-0.091}$	$1.861^{+0.174}_{-0.209}$
10408-01-29-00	$5.250^{+0.140}_{-0.132}$	$3.835^{+0.157}_{-0.233}$
20402-01-07-00	$9.201^{+0.399}_{-0.500}$	$9.584^{+0.698}_{-0.790}$
20402-01-08-00	$8.282^{+1.247}_{-1.567}$	$13.721^{+0.685}_{-0.642}$
20402-01-08-01	$8.618^{+1.253}_{-1.752}$	$13.078^{+1.037}_{-1.734}$
20402-01-10-00	$10.667^{+0.265}_{-1.159}$	$4.635^{+2.678}_{-0.869}$
20402-01-11-00	$7.977^{+0.501}_{-0.649}$	$10.268^{+0.590}_{-0.711}$
20402-01-12-00	$8.321^{+0.334}_{-0.473}$	$8.251^{+0.826}_{-0.269}$
20402-01-13-00	$11.128^{+0.161}_{-0.165}$	$8.312^{+0.411}_{-0.325}$
20402-01-14-00	$11.501^{+0.417}_{-0.745}$	$9.279^{+1.751}_{-0.869}$
20402-01-15-00	$8.221^{+0.152}_{-0.322}$	$3.170^{+1.269}_{-0.728}$
20402-01-20-00	$9.202^{+0.548}_{-1.198}$	$10.267^{+1.458}_{-1.148}$
20402-01-50-01	$3.079^{+0.041}_{-0.040}$	$0.678^{+0.190}_{-0.156}$
20402-01-51-00	$4.126^{+0.138}_{-0.040}$	$0.488^{+0.138}_{-0.104}$
20402-01-52-00	$3.812^{+0.127}_{-0.206}$	$2.773^{+0.299}_{-0.247}$
20402-01-09-00†	$9.054^{+0.829}_{-0.564}$	$8.648^{+0.935}_{-2.56}$
20402-01-16-00†	$8.318^{+1.784}_{-0.969}$	$10.529^{+0.299}_{-2.877}$
20402-01-19-00†	$7.355^{+0.596}_{-0.659}$	$5.821^{+0.299}_{-1.912}$
20402-01-21-00†	$10.971^{+0.830}_{-0.799}$	$9.143^{+1.414}_{-1.725}$

Table 4. Frequency ν_{III}, width Δ_{III} of the harmonic QPO L_{III} from the best fit to the PDS.
† 2 sigma detection.

Obs ID	$\nu_{1/2}$	$\Delta_{1/2}$
10408-01-22-01	$1.298\,^{+0.042}_{-0.042}$	$1.105^{+0.129}_{-0.119}$
10408-01-22-02	$1.255\,^{+0.057}_{-0.068}$	$0.961^{+0.207}_{-0.164}$
10408-01-23-00	$2.026\,^{+0.057}_{-0.066}$	$0.869^{+0.209}_{-0.177}$
10408-01-24-00	$1.024\,^{+0.046}_{-0.040}$	$1.012^{+0.123}_{-0.117}$
10408-01-25-00	$0.532\,^{+0.028}_{-0.041}$	$0.703^{+0.135}_{-0.106}$
10408-01-28-00	$0.492\,^{+0.024}_{-0.044}$	$0.618^{+0.168}_{-0.098}$
10408-01-29-00	$0.882\,^{+0.051}_{-0.055}$	$0.919^{+0.170}_{-0.169}$
10408-01-30-00	$1.620\,^{+0.151}_{-0.146}$	$2.229^{+0.159}_{-0.266}$
10408-01-31-00	$1.556\,^{+0.241}_{-0.307}$	$1.904^{+0.440}_{-0.430}$
20402-01-04-00	$1.594\,^{+0.065}_{-0.072}$	$1.309^{+0.146}_{-0.171}$
20402-01-07-00	$1.041\,^{+0.034}_{-0.037}$	$1.669^{+0.098}_{-0.086}$
20402-01-08-00	$1.406\,^{+0.046}_{-0.046}$	$1.866^{+0.104}_{-0.098}$
20402-01-08-01	$1.277\,^{+0.055}_{-0.062}$	$1.661^{+0.163}_{-0.134}$
20402-01-09-00	$1.346\,^{+0.024}_{-0.035}$	$0.303^{+0.150}_{-0.089}$
20402-01-10-00	$1.440\,^{+0.030}_{-0.029}$	$0.630^{+0.150}_{-0.126}$
20402-01-11-00	$1.363\,^{+0.039}_{-0.047}$	$1.872^{+0.247}_{-0.184}$
20402-01-12-00	$1.238\,^{+0.026}_{-0.027}$	$1.175^{+0.174}_{-0.138}$
20402-01-13-00	$1.575\,^{+0.021}_{-0.021}$	$1.780^{+0.061}_{-0.063}$
20402-01-14-00	$1.567\,^{+0.040}_{-0.024}$	$1.956^{+0.167}_{-0.143}$
20402-01-15-00	$1.092\,^{+0.030}_{-0.030}$	$0.325^{+0.760}_{-0.096}$
20402-01-18-00	$1.584\,^{+0.027}_{-0.025}$	$0.684^{+0.154}_{-0.119}$
20402-01-19-00	$1.077\,^{+0.022}_{-0.027}$	$0.164^{+0.124}_{-0.063}$
20402-01-20-00	$1.592\,^{+0.022}_{-0.022}$	$0.563^{+0.112}_{-0.089}$
20402-01-21-00	$1.862\,^{+0.073}_{-0.128}$	$0.806^{+0.601}_{-0.257}$
20402-01-49-00	$1.127\,^{+0.105}_{-0.134}$	$1.093^{+0.304}_{-0.254}$
20402-01-49-01	$1.316\,^{+0.052}_{-0.064}$	$1.108^{+0.209}_{-0.167}$
20402-01-50-01	$0.510\,^{+0.021}_{-0.024}$	$0.370^{+0.118}_{-0.118}$
20402-01-52-00	$0.744\,^{+0.044}_{-0.049}$	$0.442^{+0.221}_{-0.118}$

Table 5. Frequency $\nu_{1/2}$ and width $\Delta_{1/2}$ of the Lorentzian component $L_{1/2}$, from the best fit to the PDS.

Obs ID	ν_h	Δ_h
10408-01-22-01	$3.647\,^{+0.122}_{-0.169}$	$1.569^{+0.313}_{-0.278}$
10408-01-22-02	$3.398\,^{+0.121}_{-0.162}$	$1.715^{+0.333}_{-0.275}$
10408-01-23-00	$4.101\,^{+0.025}_{-0.025}$	$0.932^{+0.035}_{-0.037}$
10408-01-24-00	$2.647\,^{+0.092}_{-0.095}$	$1.151^{+0.120}_{-0.176}$
10408-01-25-00	$1.461\,^{+0.030}_{-0.066}$	$0.627^{+0.147}_{-0.088}$
10408-01-27-00	$0.571\,^{+0.019}_{-0.025}$	$0.686^{+0.089}_{-0.077}$
10408-01-28-00	$1.257\,^{+0.045}_{-0.081}$	$0.574^{+0.184}_{-0.074}$
10408-01-29-00	$2.595\,^{+0.075}_{-0.111}$	$1.400^{+0.370}_{-0.240}$
10408-01-30-00	$4.288\,^{+2.013}_{-2.607}$	$19.979^{+0.013}_{-0.052}$
10408-01-31-00	$4.831\,^{+0.237}_{-0.263}$	$5.377^{+0.242}_{-0.369}$
20402-01-04-00	$2.516\,^{+0.076}_{-0.109}$	$0.959^{+0.188}_{-0.167}$
20402-01-07-00	$4.606\,^{+0.065}_{-0.080}$	$1.261^{+0.455}_{-0.253}$
20402-01-08-00	$4.533\,^{+0.163}_{-0.173}$	$1.824^{+0.241}_{-0.364}$
20402-01-08-01	$4.776\,^{+0.095}_{-0.173}$	$1.052^{+0.549}_{-0.263}$
20402-01-09-00	$2.121\,^{+0.224}_{-0.602}$	$3.846^{+1.230}_{-0.692}$
20402-01-10-00	$1.884\,^{+0.404}_{-0.310}$	$6.567^{+0.442}_{-1.776}$
20402-01-11-00	$3.806\,^{+0.114}_{-0.447}$	$1.772^{+0.917}_{-0.328}$
20402-01-12-00	$2.842\,^{+0.172}_{-0.140}$	$3.020^{+0.709}_{-0.357}$
20402-01-13-00	$4.646\,^{+0.109}_{-0.168}$	$2.688^{+0.662}_{-0.265}$
20402-01-14-00	$4.082\,^{+0.186}_{-0.150}$	$1.889^{+0.240}_{-0.188}$
20402-01-15-00	$1.089\,^{+0.574}_{-0.105}$	$5.042^{+0.435}_{-0.399}$
20402-01-16-00	$3.612\,^{+0.340}_{-0.894}$	$3.871^{+1.698}_{-1.003}$
20402-01-18-00	$3.173\,^{+0.130}_{-0.515}$	$3.314^{+2.131}_{-0.540}$
20402-01-19-00	$1.432\,^{+0.215}_{-0.213}$	$4.392^{+0.617}_{-0.659}$
20402-01-20-00	$3.026\,^{+0.082}_{-0.183}$	$3.295^{+0.840}_{-0.423}$
20402-01-21-00	$3.533\,^{+0.860}_{-0.435}$	$4.169^{+1.912}_{-0.810}$
20402-01-49-00	$3.815\,^{+0.190}_{-0.231}$	$4.179^{+0.182}_{-0.197}$
20402-01-49-01	$4.033\,^{+0.138}_{-0.168}$	$4.061^{+0.120}_{-0.136}$
20402-01-50-01	$1.209\,^{+0.209}_{-0.268}$	$2.679^{+0.118}_{-0.180}$
20402-01-51-00	$1.662\,^{+0.067}_{-0.063}$	$0.928^{+0.132}_{-0.134}$
20402-01-52-00	$1.647\,^{+0.056}_{-0.058}$	$0.563^{+0.109}_{-0.094}$

Table 6. Frequency ν_h and width Δ_h of the Lorentzian component L_h, from the best fit to the PDS.

REFERENCES

Belloni T., 2010, in Lecture Notes in Physics, Vol. 794, The Jet Paradigm, Belloni T., ed., Springer Berlin / Heidelberg, pp. 53–84

Belloni T., Hasinger G., 1990, A&A, 227, L33

Belloni T., Klein-Wolt M., Méndez M., van der Klis M., van Paradijs J., 2000, A&A, 355, 271

Belloni T., Mendez M., King A. R., van der Klis M., van Paradijs J., 1997, ApJ, 488, L109+

Belloni T., Psaltis D., van der Klis M., 2002, ApJ, 572, 392

Castro-Tirado A. J., Brandt S., Lund N., 1992, IAU Circ, 5590, 2

Fender R., Belloni T., 2004, ARA&A, 42, 317

Fender R. P., Garrington S. T., McKay D. J., Muxlow T. W. B., Pooley G. G., Spencer R. E., Stirling A. M., Waltman E. B., 1999, MNRAS, 304, 865

Greiner J., Cuby J. G., McCaughrean M. J., 2001a, Nat, 414, 522

Greiner J., Cuby J. G., McCaughrean M. J., Castro-Tirado A. J., Mennickent R. E., 2001b, A&A, 373, L37

Greiner J., Morgan E. H., Remillard R. A., 1996, ApJ, 473, L107+

Ingram A., Done C., 2011, MNRAS, 415, 2323

Leahy D. A., Darbro W., Elsner R. F., Weisskopf M. C., Kahn S., Sutherland P. G., Grindlay J. E., 1983, ApJ, 266, 160

Markwardt C. B., Swank J. H., Taam R. E., 1999, ApJ, 513, L37

Psaltis D., 2006, in Compact stellar X-ray sources, Lewin W. H. G., van der Klis M., eds., pp. 1–38

Rao F., Belloni T., Stella L., Zhang S. N., Li T., 2010, ApJ, 714, 1065

Reig P., Belloni T., van der Klis M., Méndez M., Kylafis N. D., Ford E. C., 2000, ApJ, 541, 883

Remillard R. A., McClintock J. E., 2006, ARA&A, 44, 49

Rodriguez J., Varnière P., 2011, ArXiv e-prints

Sobczak G. J., McClintock J. E., Remillard R. A., Cui W., Levine A. M., Morgan E. H., Orosz J. A., Bailyn C. D., 2000, ApJ, 544, 993

Trudolyubov S. P., 2001, ApJ, 558, 276

van der Klis M., 1989, ARA&A, 27, 517

—, 2005, Astronomische Nachrichten, 326, 798

van der Klis R., 2006, Compact stellar X-ray sources, 39

Zhang W., Jahoda K., Swank J. H., Morgan E. H., Giles A. B., 1995, ApJ, 449, 930